Title
Time-resolved digital holographic microscopy of laser-induced forward transfer

Journal
Applied Physics B, 114(3)

ISSN
0946-2171

Authors
Ma, H
Venugopalan, V

Publication Date
2014-03-01

DOI
10.1007/s00340-013-5524-0

Published in final edited form as:
Appl Phys B. 2014 March 1; 114(3): 361–366. doi:10.1007/s00340-013-5524-0.

Time-resolved digital holographic microscopy of laser-induced forward transfer process

H. Ma[1,2] and **V. Venugopalan**[1,2,3,*]

[1] Department of Chemical Engineering and Materials Science, University of California, 916 Engineering Tower, Irvine, CA 92697-2575, USA

[2] Laser Microbeam and Medical Program, Beckman Laser Institute and Medical Clinic, University of California, Irvine, CA 92697-1475, USA

[3] Department of Biomedical Engineering, University of California, Irvine, CA 92697-2715, USA

Abstract

We develop a method for time-resolved digital holographic microscopy to obtain time-resolved 3-D deformation measurements of laser induced forward transfer (LIFT) processes. We demonstrate nanometer axial resolution and nanosecond temporal resolution of our method which is suitable for measuring dynamic morphological changes in LIFT target materials. Such measurements provide insight into the early dynamics of the LIFT process and a means to examine the effect of laser and material parameters on LIFT process dynamics.

1 Introduction

Laser induced forward transfer (LIFT) is a noncontact deposition method that uses focused laser microbeam irradiation to transfer thin layer of materials, patterned at high resolution, to a receiver. In the original LIFT process, the source material was a thin metal layer coated on a transparent substrate [1]. In recent years, LIFT has been used to transfer a wide variety of materials including metal oxides, superconductors, and biomaterials. Some sensitive materials are subject to thermal and mechanical damage during the traditional LIFT process. In order to overcome these potential limitations, many variations of the original LIFT technique have been developed [2]. One of the most widely used techniques is LIFT with a dynamic release layer (DRL), which employs a thin absorbing sacrificial layer between the transfer material and the donor substrate. The DRL is vaporized during the transfer by the laser irradiation which propels the top transfer material layer towards the acceptor.

One important application of LIFT is its use for the separation and transport of biological materials such as live cells [3–5]. The transfer of live cells imposes a few special requirements including: (a) material biocompatibility; (b) cell incubation in culture medium during transfer; (c) substrate biocompatibility; and (d) transport dynamics that preserve cell viability and function. For these purposes, a related technology named laser microdissection

Phone number: +1-949-824-5802 *Fax number:* +1-949-824-2541 vvenugop@uci.edu.
**Present address:* University of California, 916 Engineering Tower, Irvine, CA 92697-2575, USA

and pressure catapulting (LMPC) was developed [6–8]. LMPC consists of a laser microdissection process to separate the sample mounted on a UV-absorbing polymer foil by a focused UV laser beam, and a laser induced forward transfer process to catapult the dissected sample into the acceptor. While commonly used for excised tissue specimens, there are several possible sources for damage when using LMPC with live cells, including thermal exposure, UV irradiation, mechanical stress and desiccation during collection.

Over last several years, a novel LIFT approach has been developed to separate live, adherent cells using polymer micropallet arrays [9–11]. These micropallets are fabricated on top of a glass substrate using photolithographic methods. The cells are cultured on top of these micropallet elements, any one of which can be subsequently released by pulsed laser microbeam irradiation focused near the interface between the micropallet element and the glass substrate. One important differences between micropallet method and other LIFT processes is the absence of an acceptor. The cells are released together with the micropallet into the culture media and collected later by various strategies such as gravity [10] and magnetic forces [12, 13]. The area of each micropallet matches the sample size, and the thickness is typically 30–50 μm. The micropallet thickness is much larger than the polymer foil used in LMPC method which provides better isolation and protection from the thermal and mechanical transients produced by the pulsed laser microbeam irradiation.

Nevertheless, the use of non-optimal irradiation and material parameters in micropallet LIFT processes can compromise cell viability [14]. First, cellular exposure to high fluid shear stress during the release can have deleterious effects [15, 16]. Second, the deformation of the micropallet can result in the application of flexural stresses on the attached cells. Many studies have shown that such stresses can modulate many cellular processes [17, 18]. The ability to directly measure the dynamic deformation and motion of LIFT target with high resolution will enable detailed mechanistic studies that examine how material and laser irradiation properties might a ect damage of the transfer material in LIFT processes.

Various time resolved imaging methods, such as shadowgraphy and schlieren photography, have been used to study the dynamics of traditional LIFT processes [19–24]. In previous work [14], we measured the displacement of released micropallets using a time-resolved heterodyne interferometer [25]. As compared to numerous studies that examine the dynamics of released objects using LIFT, studies examining surface deformation during the LIFT process is relatively rare. Although the morphological dynamics during laser ablation is important in some applications [26–31], a limited variety of metrological methods that have been applied. Brown and co-workers employed side view time resolved images to study the blister formation during blister-actuated laser induced forward transfer (BA-LIFT) [30]. The sensitivity of this method depends on the numerical aperture (NA) of the imaging objective lens, and can not exceed the image resolution. Moreover, this method assumes axial symmetry since a full two-dimensional deformation field cannot be acquired. Furutani and co-workers used a time-resolved interferometry method for their laser-induced ablation dynamics study [26, 27]. This interferometric approach is more sensitive in the vertical direction than the side view imaging approach of Brown. However, in Furutani's method, the surface deformation was obtained by simply observing the fringe movement. Therefore, the

measurement does not provide quantitative deformation and is only sensitive in the direction perpendicular to the orientation of the linear fringe pattern.

Holography is widely used measurement of three-dimension surface profile measurement. The rapid development of digital solid state sensors and computers has made digital holography increasingly attractive for its convenient and fast processing compared to the traditional holographic plate method. Furthermore, unlike the phase-shifting interferometry, the quantitative phase can be reconstructed numerically from a single hologram in digital holography [32, 33]. These characteristics makes digital holography an attractive approach to measure the deformation in transient events.

In this work, we develop a time-resolved digital holographic microscopy method to study the dynamic deformation of LIFT process. We measure the top surface deformation of micropallets during the LIFT, and compare the results to interferometric displacement measurements obtained in a previous study [14]. These results offer complementary information regarding the dynamics of released micropallets and provides important insights necessary to assess the cellular exposure to mechanical stresses during the release procedure. More generally, this work demonstrates a new approach to study dynamic deformation associated with early stages of LIFT processes.

2 Material and Methods

2.1 Micropallet array

The micropallet arrays are identical to those used in our previous study [14]. The square pallets are fabricated using 1002F photoresist polymer on a 0.9 mm thick BK-7 glass slide. The dimension (L × W × H) of each pallet is 100 × 100 × 50 μm with 20 μm spacing between adjacent pallet elements. The top surface of the pallets is coated with an 80% dielectric reflective coating, which reduces the back reflection from the bottom surface while providing sufficient transmission for bight-field imaging. In our interferometric pallet release measurements [14], both the pallets and probe beam focusing lens were immersed in water. However, in this holographic measurement, a low magnification lens is needed for a reasonable field of view. Since a low magnification water immersion objective lens was not readily available, we fabricated a custom small water chamber with the micropallet array as the bottom. The chamber is covered with a 200 μm thick cover glass, which is coated with anti-reflective coating for maximum transmission. The water is filled between the micropallet array bottom and the cover glass.

2.2 Optical system

A schematic of the digital holographic microscopy system is shown in Fig. 1. Micropallets are released using the emission from an ablation laser which is passively Q-switched diode pumped solid state (DPSS) laser (Power-chip PNG-M, Teem Photonics, France) providing 500 ps duration laser pulses at λ = 532 nm. The laser beam is expanded to overfill the back aperture of the focusing objective lens to obtain a near diffraction-limited focal volume. The laser beam is attenuated by a half-wave plate and a polarizing beam splitter. The laser pulse energy is measured by inserting an photodetector (EPM1000 with J5-09 sensor, Coherent

Inc., Santa Clara, CA, USA) into the beam path immediately before the beam enters the side port of the inverted microscope (IX-81, Olympus America, Center Valley, PA, USA). Once the ablative laser beam enters the microscope housing, it is reflected by a dichroic beam splitter and then focused by a microscope objective lens (LUCPLFLN 20×/0.45, Olympus America) near the interface between the polymer micropallet and the glass substrate. The height of the focal volume can be controlled by adjusting the vertical position of the microscope objective lens. The micropallet array is placed on a automated XY stage (MS-2000, Applied Scientific Instrumentation, Eugene, OR, USA) so that the micropallet element to be released can be precisely centered in the field of view.

A holographic microscope system based on Mach-Zehnder interferometer is used to detect the deformation of the top surface of the micropallets. The probe light source is a flashlamp-pumped, Q-switched, frequency-doubled Nd:YAG laser (SL332, EKSPLA, Vilnius, Lithuania) emitting 1100 ps duration pulses at λ = 532 nm. The laser output is focused by a positive lens L1 and then filtered by a 40 μm pinhole to clean up the spatial mode. The filtered beam is subsequently collimated by lens L2. The collimated beam is split using a polarizing beam splitter (PBS). The transmitted beam is used as the reference, while the reflected beam is used as the probe beam to detect the surface profile of the pallet. The reflection to transmission ratio of the PBS is controlled by rotating the beam polarization with a half-wave plate before PBS. In this way, we can balance the optical intensity of the two arms of the interferometer to maximize the contrast in the interferogram. The probe beam is focused by a microscope objective lens (Plan N 4×/0.10, Olympus America), which is used as both condenser lens for illumination and imaging lens for holography. This 4× objective lens is mounted on the microscope condenser lens holder with a custom-made adapter, so the holography objective lens can be adjusted in XYZ directions using the microscope condenser lens mount. In the reference arm, a pair of mirrors are mounted on a linear translation stage to adjust the optical path of the reference arm to match that of the sample arm. A half-wave plate is placed in the reference beam path to rotate the polarization of the reference beam by 90° in order to align the polarizations of two interfering beams. The interferogram is recorded by a CCD camera (ORCA-R2, Hamamatsu Photonics K.K., Japan) for data processing.

The ablation laser is focused near the center of the bottom surface of the micropallet. After focusing at the polymer-glass interface, the ablation objective lens is raised by 6 μm as this is the focus height that accomplishes pallet release using the lowest pulse energy [14]. The pulse energy of the ablation laser is set to 3.5 μJ, which provides consistent pallet release. The probe laser beam and the holography objective lens are adjusted carefully, such that the focused probe beam is centered precisely on the micropallet to be released while it is reflected back along the optical axis by the micropallet array. The holography objective lens is adjusted in the axial direction until a magnified real image of micropallets is formed at a distance. In our experiments, the image plane is about 700 mm behind the camera sensor plane. Off-axis holography is employed here, so the reference beam is intentionally steered by a small angle relative to the probe beam. The reference beam and the reflected probe beam have full overlap area in the camera sensor plane, while they are separated spatially at a distance.

The timing of the ablation laser, probe laser, and camera is controlled by a digital delay generator (575 series, Berkeley Nucleonics Corp., San Rafael, CA, USA). The actual delays are monitored by a digital oscilloscope (TDS2024, Tektronix Inc., Beaverton, OR, USA).

2.3 Holography reconstruction

The amplitude and phase of the optical wave are reconstructed numerically from the off-axis hologram by a computer. The surface deformation can be calculated from the phase-contrast image because there is a linear mapping between phase and deformation. The amplitude-contrast image enables visualization of the sample in order to find the location of the real image during reconstruction. This image also allows clear identification of the micropallet boundaries, which is often difficult in the phase-contrast image due to the phase corruption caused by sharp sidewall slope and refractive index mismatch of the pallet elements.

Holographic reconstruction is performed using the method described by Cuche and co-workers [32]. The hologram is multiplied by a computed replica of the reference wave, which is a plane wave in our case. The diffraction pattern of the hologram is calculated using Fresnel transform at a distance d from the hologram plane. When d equals the distance between the CCD sensor and the real image during the hologram recording, the calculated diffraction pattern shows the best amplitude-contrast image of the pallet. In practice, we use this method to find the optimum value of d. This procedure imitates the focusing in traditional optical microscopy. The phase-contrast image is more complicated because the real image during recording contains quadratic phase factors introduced by the holography objective lens [34]. The quadratic phase factors do not a ect the intensity distribution in the image plane, but they will distort the phase-contrast image. Cuche and co-workers proposed a digital method to correct this distortion [32]. A computed complex conjugate of the quadratic phase factors can be multiplied with the reconstructed wave to compensate for this aberration. We adopt this method in our experiment. The quadratic phase curvature is found experimentally by minimizing the non-uniformity and curvature in the wrapped phase-contrast image of a flat object.

The holograms are recorded before and after the ablation laser is fired. The reconstructed phase-contrast images obtained prior to the delivery of the ablation laser microbeam are subtracted from the phase-contrast images acquired at a fixed time point following laser microbeam irradiation to obtain the relative phase shift and to remove the additional phase errors. The obtained phase is unwrapped using Goldstein's algorithm [35]. The deformation (z) of the top pallet surface is calculated pixel-wise from the unwrapped phase using $z = \lambda\Phi(4\pi n)$, where λ is the wavelength in air, Φ is the unwrapped phase, and n is the refractive index of water. The standard deviation of z is reduced to less than 4 nm after the phase correction and subtraction.

3 Results and Discussion

Typical amplitude-contrast and phase-contrast images of the released micropallets at three delay times are shown in Figure 2. At 52 ns following laser microbeam irradiation of the pallet (Figures 2a and 2b), the polymer material is vaporized and the vapor is confined in the closed volume near the interface between the polymer micropallet and the glass substrate.

This confined ablation process causes the top surface of the micropallet to bulge out at its center. At 405 ns (Figures 2c and 2d), the vapor has percolated through the glass-pallet interface and begins to leak out from under the pallet on one side. This vapor leakage causes the location of maximum vertical displacement to shift from the pallet center to the periphery. The phase of the image close to the location of this vapor leakage tends to be corrupted because the escaping vapor provides a sharp refractive index discontinuity. At these time points, the pallet remains attached to the substrate overall, even though vapor is present between the pallet and the glass substrate. At 1350 ns (Figures 2e and 2f), pallet detaches and begins to release. Once this occurs, the forces that created the pallet deformation disappear, and the entire pallet element is tilted upward. Complete release occurs in this stage and the actual release time depends on the adhesion between the polymer pallet and the glass substrate, which varies from pallet to pallet [14].

Even with these pallet to pallet variations, the early deformation dynamics are very consistent. To validate the these digital holographic microscopy measurements, we compare them to measurements obtained using heterodyne interferometry that provide continuous time-resolved records of pallet motion at a single location on the pallet surface [14, 25]. In the heterodyne interferometry measurements, the probe laser was focused to a small area at the center of the pallet with a diameter corresponding to one quarter the micropallet size. To compare these measurements with the holography data we need to obtain the displacement of this central portion of the pallet from the holographic images. Unfortunately, absolute displacement values cannot be obtained from the digital holographic measurement because the phase is corrupted at the border of the pallet. However, we do know that the pallet is not fully released at the early stages and so the displacement of the central part can be calculated from its height relative to peripheral pallet locations which experience no motion at these early stages of the LIFT dynamics. The height of the central part is calculated by averaging the deformation in a 10×10 pixel region at the pallet center, which matches the area of the focused laser beam used in the heterodyne interferometry measurements. The low reference height is calculated by averaging the height in a 3×3 pixel area in one of the pallet corners. The pallet displacement calculated from the holographic data is plotted in Figure 3 together with the heterodyne interferometry data. The two data sets were obtained in different experimental trials but were obtained using the same laser microbeam pulse energy (3.5 μJ) and focusing conditions. We use a spline curve to connect the data points which demonstrates broad agreement between the two measurements.

From Figure 3, we can see that the holographic measurement matches the heterodyne interferometric data very well. The minor differences can be attributed to two primary factors. Firstly, the temporal sampling interval of the holographic data is from several nanoseconds to several tens of nanoseconds, which is much larger than the 0.2 nanoseconds sampling interval of the heterodyne interferometry measurements. Therefore, the curve fitted from holographic data lacks some temporal details and can be distorted due to the larger sampling time. Secondly, each time point for time-resolved holographic data is obtained from the release of a different pallet. Although the early stage dynamics of the released pallet is very consistent, some pallet-to-pallet variation can still be expected.

4 Conclusions

We have developed and demonstrated a digital holographic microscopy system to provide a wide-field imaging method to visualize early stages of LIFT process with nanometer axial resolution and nanosecond temporal resolution. Comparison of the holographic deformation data with independent measurements obtained using heterodyne interferometric data shows very good agreement. The lateral resolution of the system depends on the NA of the holographic imaging lens. In our experiment, a low NA objective lens was used to obtain a relatively large field of view. In high NA applications, sub-micrometer resolution can be obtained within the visible spectral region.

The high resolution of the digital holographic microscopy improves upon the imaging methods used in previous studies on surface morphology dynamics of LIFT processes [26, 27, 30]. Furthermore, the digital holographic microscopy provides quantitative deformation over the full area of interest. This is in contrast with previous approaches only provided the deformation along a particular direction within the area of interest. This capability enables us to analyze complicated surface deformation in addition to simple deformation with certain symmetries.

Acknowledgments

We acknowledge support from the National Institutes of Health (NIH) via R01 HG004843. We also acknowledge support of the Laser Microbeam and Medical Program, a NIH Biomedical Technology Resource via P41-EB015890.

References

1. Bohandy J, Kim BF, Adrian FJ. Journal of Applied Physics. 1986; 60:1538.
2. Arnold CB, Serra P, Piqué A. MRS Bulletin. 2007; 32:23.
3. Hopp B, Smausz T, Antal Z, Kresz N, Bor Z, Chrisey D. Journal of Applied Physics. 2004; 96:3478.
4. Doraiswamy A, Narayan R, Lippert T, Urech L, Wokaun A, Nagel M, Hopp B, Dinescu M, Modi R, Auyeung R, et al. Applied Surface Science. 2006; 252:4743.
5. Ringeisen BR, Kim H, Barron JA, Krizman DB, Chrisey DB, Jackman S, Auyeung R, Spargo BJ. Tissue Engineering. 2004; 10:483. [PubMed: 15165465]
6. Schütze K, Lahr G. Nature Biotechnology. 1998; 16:737.
7. Stich M, Thalhammer S, Burgemeister R, Friedemann G, Ehnle S, Lüthy C, Schütze K. Pathology - Research and Practice. 2003; 199:405.
8. Horne er V, Linz N, Vogel A. Journal of Biomedical Optics. 2007; 12:054016. [PubMed: 17994904]
9. To'a Salazar G, Wang Y, Young G, Bachman M, Sims CE, Li GP, Allbritton NL. Analytical Chemistry. 2007; 79:682. [PubMed: 17222037]
10. Wang Y, Young G, Bachman M, Sims CE, Li, Allbritton NL. Analytical Chemistry. 2007; 79:2359. [PubMed: 17288466]
11. Salazar GT, Wang Y, Sims CE, Bachman M, Li GP, Allbritton NL. Journal of Biomedical Optics. 2008; 13:034007. [PubMed: 18601552]
12. Gunn NM, Chang R, Westerhof T, Li G-P, Bachman M, Nelson EL. Langmuir. 2010; 26:17703. [PubMed: 20968293]
13. Gach PC, Sims CE, Allbritton NL. Biomaterials. 2010; 31:8810. [PubMed: 20719380]
14. Ma H, Mismar W, Wang Y, Small DW, Ras M, Allbritton NL, Sims CE, Venugopalan V. Journal of The Royal Society Interface. 2012; 9:1156.

15. Rau KR, Quinto-Su PA, Hellman AN, Venugopalan V. Biophysical Journal. 2006; 91:317. [PubMed: 16617076]
16. Hellman AN, Rau KR, Yoon HH, Venugopalan V. Journal of Biophotonics. 2006; 1:24. [PubMed: 19343632]
17. Wang Y, Botvinick EL, Zhao Y, Berns MW, Usami S, Tsien RY, Chien S. Nature. 2005; 434:1040. [PubMed: 15846350]
18. Geiger B, Bershadsky A. Cell. 2002; 110:139. [PubMed: 12150922]
19. Papazoglou DG, Karaiskou A, Zergioti I, Fotakis C. Applied Physics Letters. 2002; 81:1594.
20. Fardel R, Nagel M, Nuesch F, Lippert T, Wokaun A. The Journal of Physical Chemistry C. 2010; 114:5617.
21. Young D, Auyeung RCY, Piqué A, Chrisey DB, Dlott DD. Applied Physics Letters. 2001; 78:3169.
22. Hopp B, Smausz T, Kresz N, Barna N, Bor Z, Kolozsvári L, Chrisey DB, Szabó A, Nógrádi A. Tissue Engineering. 2005; 11:1817. [PubMed: 16411827]
23. Nakata Y, Okada T. Applied Physics A: Materials Science & Processing. 1999; 69:S275.
24. Zergioti I, Karaiskou A, Papazoglou D, Fotakis C, Kapsetaki M, Kafetzopoulos D. Applied Surface Science. 2005; 247:584.
25. Carp SA, Guerra A III, Samuel J, Duque Q, Venugopalan V. Applied Physics Letters. 2004; 85:5772.
26. Furutani H, Fukumura H, Masuhara H. Applied Physics Letters. 1994; 65:3413.
27. Furutani H, Fukumura H, Masuhara H, Lippert T, Yabe A. The Journal of Physical Chemistry A. 1997; 101:5742.
28. Willis DA, Grosu V. Applied Surface Science. 2007; 253:4759.
29. Kattamis NT, Purnick PE, Weiss R, Arnold CB. Applied Physics Letters. 2007; 91:171120.
30. Brown MS, Kattamis NT, Arnold CB. Journal of Applied Physics. 2010; 107:083103.
31. Kattamis NT, Brown MS, Arnold CB. Journal of Materials Research. 2011; 26:2438.
32. Cuche E, Marquet P, Depeursinge C. Applied Optics. 1999; 38:6994. [PubMed: 18324243]
33. Kreis, T. Handbook of Holographic Interferometry. Wiley-VCH Verlag GmbH & Co. KGaA; 2005. ISBN 9783527405466
34. Goodman, JW. Introduction To Fourier Optics. Roberts & Company Publishers; 2005. ISBN 0974707724
35. Ghiglia, DC.; Pritt, MD. Two-Dimensional Phase Unwrapping. John Wiley & Sons, Inc.; 1998. ISBN 9780471249351

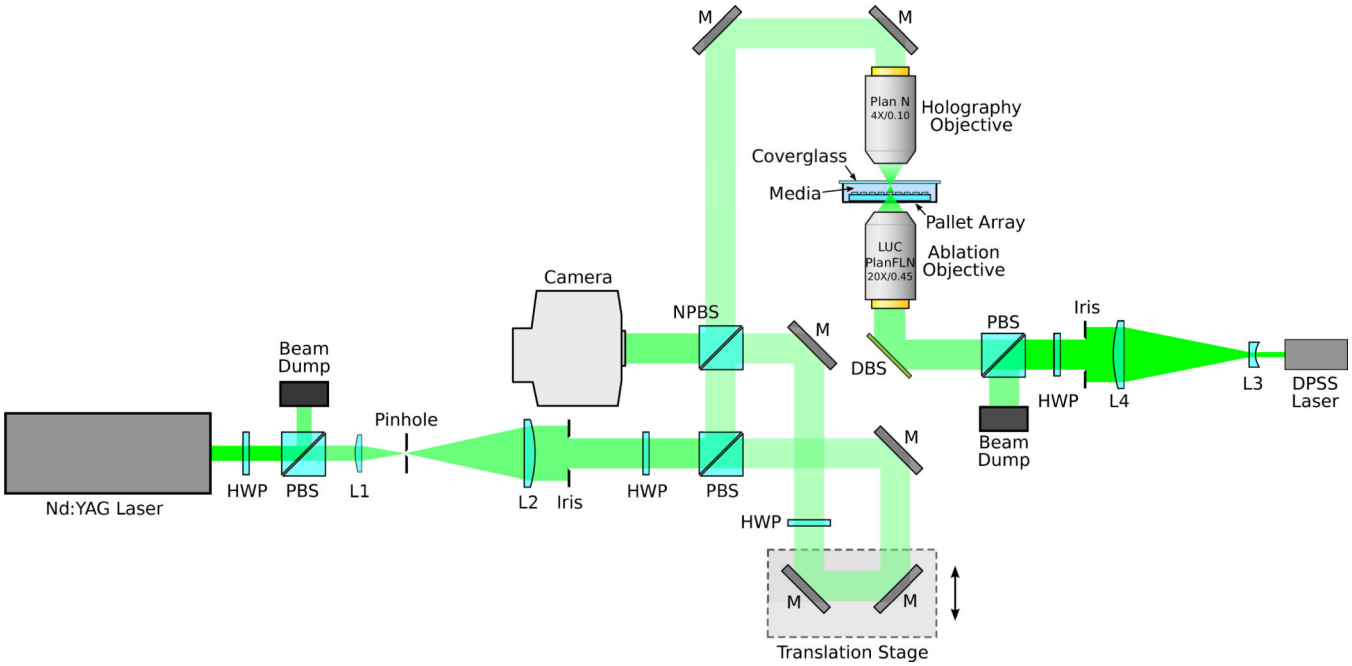

Fig. 1.

Schematic of the time-resolved digital holographic microscope system. HWP: half-wave plate; PBS: polarizing beam splitter; NPBS: non-polarizing beam splitter; DPS: dichroic beam splitter; M: mirror; L1, L2, L3, L4: lenses. The focal lengths of L1, L2, L3, L4 are 200 mm, 500 mm, −25 mm, and 500 mm, respectively.

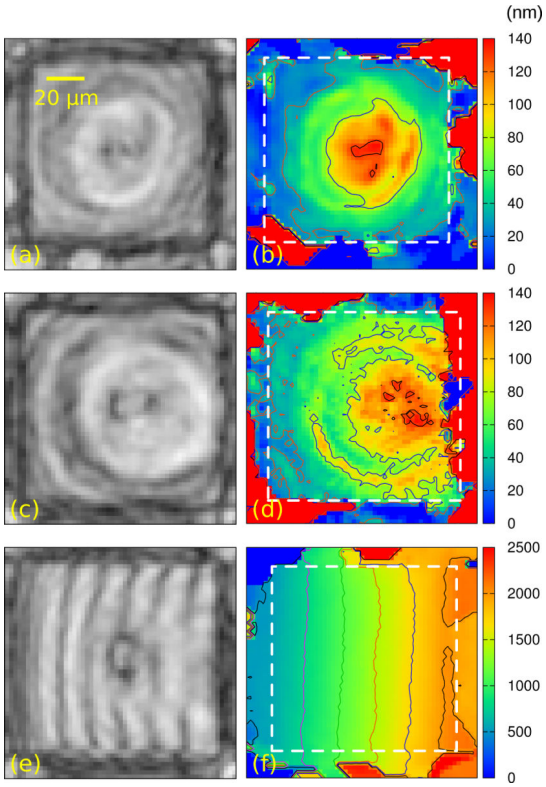

Fig. 2.

Reconstructed amplitude (a, c, and e) and deformation (b, d, and f) images of pallets at three different time delays: 52 ns (a and b), 405 ns (c and d), and 1350 ns (e and f). The interval between adjacent contour levels in the deformation figures are 50 nm (b), 50 nm (d), and 300 nm (f) respectively. The white dashed squares show the border of each pallet.

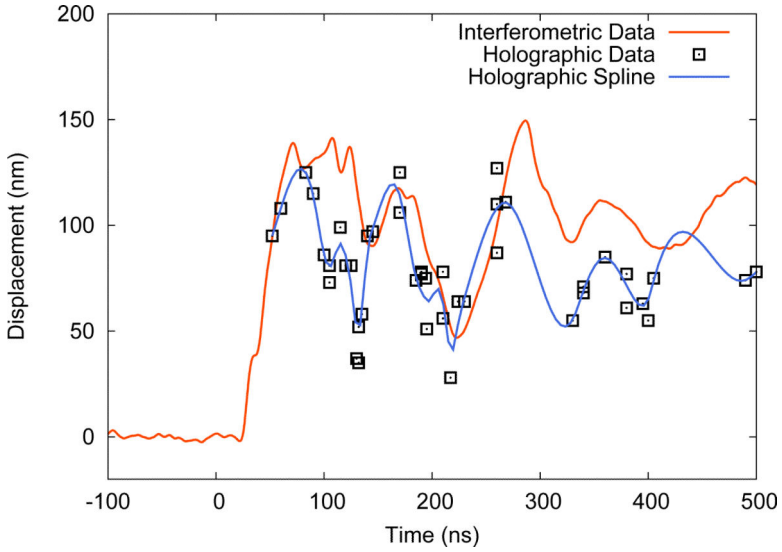

Fig. 3.

The displacement of the central part of pallets prior to release. The red curve shows the result of heterodyne interferometry measurements [14]. The black boxes shows the digital holographic microscopy data. The blue curve is a spline curve fitted to the holographic data.